Journal of Alloys and Compounds 504 (2010) 76–82

Contents lists available at ScienceDirect

Journal of Alloys and Compounds

journal homepage: www.elsevier.com/locate/jallcom

Structure–property correlation in cellular silica processed through hydrophobized fused silica powder for aerospace application

Sarika Mishra[a,*], R. Mitra[b], M. Vijayakumar[c]

[a] Non Ferrous Materials Technology Development Centre, Hyderabad 500 058, India
[b] Indian Institute of Technology, Kharagpur 721 302, India
[c] Defence Metallurgical Research Laboratory, Hyderabad 500 058, India

ARTICLE INFO

Article history:
Received 18 March 2010
Received in revised form 6 May 2010
Accepted 7 May 2010
Available online 20 May 2010

Keywords:
Porosity
Mechanical properties
Optical microscopy
Silica foam

ABSTRACT

Attempts have been made towards a novel process for the preparation of cellular silica with interconnected cells, tailored porosity and pore size distribution using a combination of hydrophobized fused silica powder and direct foaming methodology. The process has resulted into cellular silica tiles as large as 100 × 100 × 25 mm dimensions. The resulting ceramic foams sintered at 1100 °C, consisted of a highly interconnected network of spherical cells with densities as low as 10% of theoretical. The pore size distributions and cell size have been found in the range of 50–250 μm and ~6–16 ppi, respectively. The microstructure has shown an open and interconnected porosity with an average permeability occurring in the region of $\sim 10^{-8}$ m^2. The creation of highly densified cell walls and tortuous struts between the cells has led to foams with a comparatively high compressive strength and Young's modulus and with an excellent thermal shock properties.

1. Introduction

Cellular silica with improved framework, crosslinking and stability properties are desirable for thermal protection systems (TPS) in aerospace applications [1,2]. In general, the properties such as permeability, thermal conductivity, mechanical behavior and dielectric strength, depend on the volume fraction of porosity and microstructure of the ceramic foams. However, silica is a well-known material for its brittleness and low strength. One of the most significant usages of amorphous silica (quartz) fibers is in the thermal protection system of the re-entry vehicles [3]. The silica fibers used for making these tiles are either drawn from fused quartz melts or made by leaching of high quality glass fibers using a tedious and environmentally unfriendly process, thereby increasing the cost of fibers. Hence, a different approach involving the application of a foam casting route for fabricating the protective tiles using the fused silica powder instead of fibers has attracted considerable attention in recent years.

Among the several known processes for production of foams [4–8], the *direct foaming method* [9] is one of the simplest ways of introducing pores in ceramic foams. In this process, the foams are prepared by incorporating air into a suspension by a controlled mechanical operation, followed immediately by casting of the foam, as well as subsequent drying and sintering under optimized conditions. One critical step in this process is the consolidation of the foam after casting. Here is where particle-stabilized foams are very advantageous, since the consolidation can be skipped due to the formation of a network of particles between bubbles. The major advantage with this process is that the structure of air bubbles created during foaming is undisturbed till the sintering is complete. This is true only if the bubbles are stable enough to prevent Ostwald ripening and coalescence. The total porosity in such foams is proportional to the amount of air incorporated in the suspension during the foaming process. The process has shown several advantages over widely used injection moulding process using ceramic powder-thermoplastic polymer blends. For example, the pourable suspensions are easy to handle for mould filling when compared to the hot viscous systems those used in the injection moulding process. In addition, the direct foaming process allows the binder to be used in small quantities and thereby avoids long and complicated binder burnout schedule.

This paper presents the results of a study on the process–structure–property relationship of porous silica tiles as large as 100 × 100 × 25 mm, prepared by foam casting method. The detailed outcome of hydrophobized fused silica dispersions on the foam development behavior has been examined and the effect of the foaming process on the resultant microstructure, mechanical and thermal properties towards end use application has been discussed.

* Corresponding author. Tel.: +91 40 24341332; fax: +91 40 24342567/2300.
E-mail address: uptecsarika@rediffmail.com (S. Mishra).

0925-8388/$ – see front matter © 2010 Elsevier B.V. All rights reserved.
doi:10.1016/j.jallcom.2010.05.056

2. Experimental details

2.1. Raw materials

The raw materials used in this study include fused silica powder (Industrial grade, d_{50} = 10 μm), alumina powder (Industrial grade, d_{50} = 0.70 μm), cetyl trimethyl ammonium bromide, CTAB (CR grade, S.D. Fine Chemicals Ltd.) as cationic dispersant, and polyvinyl alcohol (PVA, molecular weight = 1,25,000, Fischer, LR grade), sucrose (LR grade, S.D. Fine Chemicals Ltd.), colloidal silica (pH 8.8, particle size = 27.3 nm, silica content = 40%) as binders.

2.2. Foam casting

The processing of silica foams was carried out in several steps. The first step in foam casting was ball milling the fused silica powder with 5 wt.% alumina and 0.05% CTAB for 100 h using alumina milling media of 8–10 mm diameter in 1:1 ratio. This ball-milled precursor powder mixture was used for processing of silica foams. The second step involved the preparation of aqueous silica suspensions by pot milling the constituents at 30 rpm speed in polypropylene containers for 2 h. The green strength of the foams was optimized through careful selection of solid loading in the range of 25–35%, binder constituents including 2–4 vol.% PVA, 10–30 vol.% sucrose, as well as 5 vol.% colloidal silica in various combinations. The third step comprised the foaming operation. The milled slurry was then put on the roller mill at a speed of 30 rpm, and subjected to foaming for 2–4 h by entraining air into the suspension. In addition, orientation of the bottle in the roller mill was changed to a position orthogonal with respect to the previous, so that the slurry could move along the length of the bottle and access a larger volume of air. In the fourth and fifth steps, the foamed suspensions were then cast into petroleum jelly coated suitable perspex moulds. During casting, the mould was periodically tapped to distribute the foam uniformly. The sixth step involved controlled drying of the cast foams (T = 30 °C, relative humidity = 40–80%, Osworld Humidity Chamber) in a graded fashion, followed by drying in a convection oven at temperatures up to 100 °C in steps. In the seventh and final step, the fully dried samples were subjected to binder burn-out followed by sintering at 1100 °C, which was reached at a heating rate of 1 °C/min.

In order to prevent the foams from erosion during handling and usage, the surface needs to be densified and strengthened. For this purpose, a silica slurry with very low solid loading was prepared in aqueous medium with guar gum (0.2–0.5 wt.%) and colloidal silica (5 vol.%) as binder, using precursor powder. The slurry was thoroughly mixed for 24 h, and then applied as a thin coating on all surfaces of the porous green body having dimension of 100 × 100 × 25 mm. The coated sample was slowly dried up to 110 °C in an air oven. The surface densified and dried porous silica tile thus prepared was sintered at 1100 °C. The detailed methodology for making hydrophobized silica foams has been described elsewhere [10].

2.3. Characterization

The rheological behavior of the as prepared fused silica suspensions was examined using a rotary viscometer in parallel plate configuration (40 mm diameter, 1 mm gap) with a solvent trap (Model AR1000, TA Instruments, New Castle, DE). The measurements were performed at room temperature (27 °C) at shear rates varying from 0.5 to 50 s^{-1} prior to the foaming step. The samples were characterized for their green and sintered density by the Archimedes principle, using kerosene (ρ = 0.798 g/cc) as the solvent.

The microstructure of ceramic foams was characterized quantitatively through optical microscopy, using the image analysis software (Image Tool, version 3.0) and scanning electron microscopy (SEM) (Leo 440i, UK). In addition, the pore size distribution was characterized through mercury porosimetry (Quantachrome Poremaster, version 4.01). The room temperature air permeability of the sintered disks with 25 × 25 × 8 mm size was determined by measuring the pressure drop across the sample as a function of the gas flow rate. The experimental set-up was prepared following ASTM C 577-99 standard [11] for measuring the air pressure drop across the sample as a function of the gas flow rate.

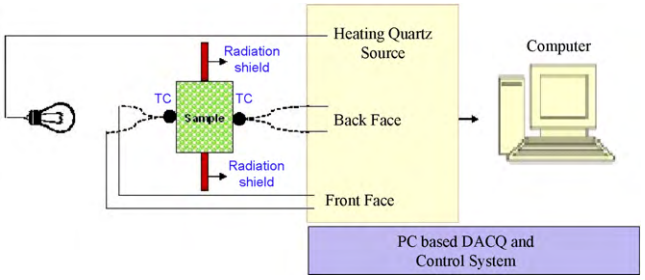

Fig. 1. Schematic representation of the experimental set-up for thermal analysis of porous silica tiles.

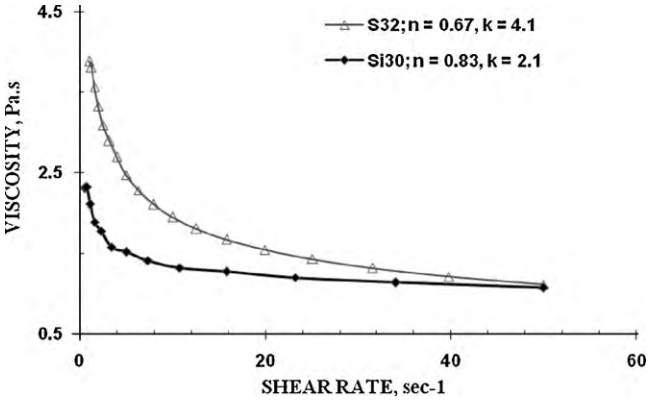

Fig. 2. Plot showing the variation of viscosity with shear rate for silica slurry.

For compression tests, the samples were drilled to dimensions of 9.25 mm dia. and 18 mm height using ultrasonic drilling machine. The foams were compression tested (Instron 5501R UTM), following the method used by Brezny and Green [12]. The aluminum spacers of 9 mm dia. and 5 mm height were fixed to both the flat ends of cylindrical samples so that load transfer to the samples was uniform. Furthermore, the static elastic modulus was estimated from the slope of the elastic part of stress–strain curve. The Gibson Ashby approach [Eq. (1)] to describe the compression strength (σ_{fc}) and Young's modulus, of the *open cell*, brittle materials as a function of density and cell size has been used to calculate the geometric constant, C_i and the property dependent exponent, n of silica foams.

$$\frac{\sigma_{fc}}{\sigma_{fs}} = C_i \left(\frac{\rho}{\rho_s}\right)^{3/2} \quad (1)$$

where ρ/ρ_s is the relative density (ρ is density of the foam and ρ_s is the theoretical density of strut material) and σ_{fs} is the fracture strength of the strut.

The thermal properties of the coated [10] and sintered silica tile (100 × 100 × 25 mm size; 85% porous), was recorded through an indigenous set-up shown in Fig. 1. For testing purpose, the silica tile was painted black on one of its surfaces (front face). Both the front and back surfaces of the tile were instrumented to separate thermocouples. The front face of the panel was exposed

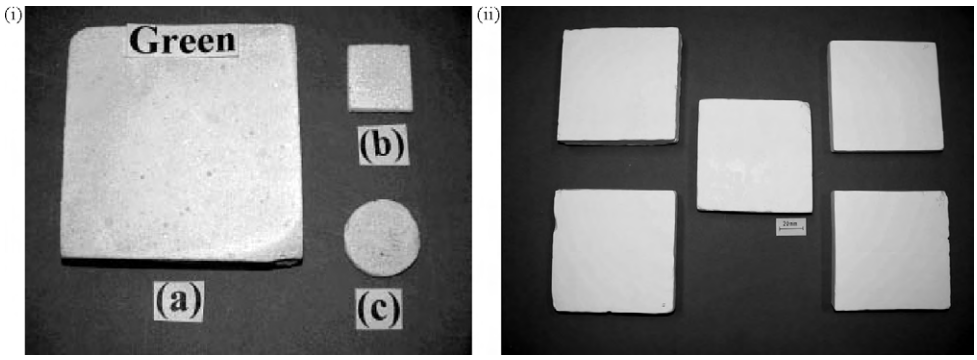

Fig. 3. (i) Photographs of green samples, dried at 110 °C: (a) a typical, 100 × 100 × 25 mm panel; (b) a square disc and (c) a round disc cut from the panel. (ii) Surface densified sintered porous silica tiles of 100 × 100 × 25 mm dimensions.

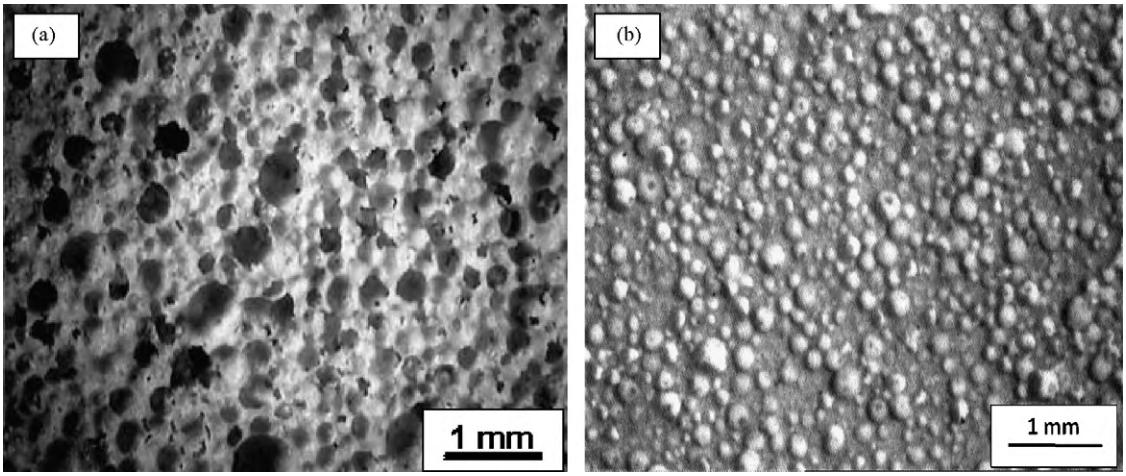

Fig. 4. Optical micrographs of sintered silica foams with RD of: (a) 0.11 and (b) 0.20.

to radiant energy through a continuous heating source or flash comprising a set of quartz lamps. The rate of heating pulse was kept as high as ~40 °C/s and the temperature on the other surface (rear face) was recorded. The front and back face temperatures were then plotted as a function of time.

The thermal profile of silica tile was measured using 1D time marching solution simulating thermal shock by heating one surface at a rapid rate. The calculations were done using a one-dimensional (1D) Time Marching solution assuming different thermal diffusivities and time interval of 2 s generated different back face temperature profiles using formula $\alpha = dT/dt$, where α is the thermal diffusivity, T is the back face temperature (in °C) and t is time (in seconds). This model consisted of calculated curves of different thermal diffusivities for assessing the thermal diffusivity of the porous sample. The experimental curve for the back face temperature profile was fitted into this model to obtain the thermal diffusivity for porous silica tile (RD = 0.15). The thermal conductivity (λ) was then obtained using Eq. (2):

$$\lambda = \alpha \rho c \quad (2)$$

where ρ is the density and c is the specific heat of the material.

The Young's modulus (Dynamic Elastic Properties Analyzer, DEPA, Jagdish Electronics, Bangalore, India) of the porous silica tiles was determined before and after their thermal exposures to assess the damage caused by thermal shock.

3. Results and discussions

3.1. Slurry rheology

Fig. 2 shows the plot for variation of viscosity with shear rate for silica slurry. The slurry shows shear thinning (viscoelastic) behavior, very typical of such highly loaded slurries [13]. Such a behavior is critical for the processing methodology adopted, as it ensures that the mixing and foaming operations occur during the low viscosity regime because of the shearing action associated with the ball-milling operation.

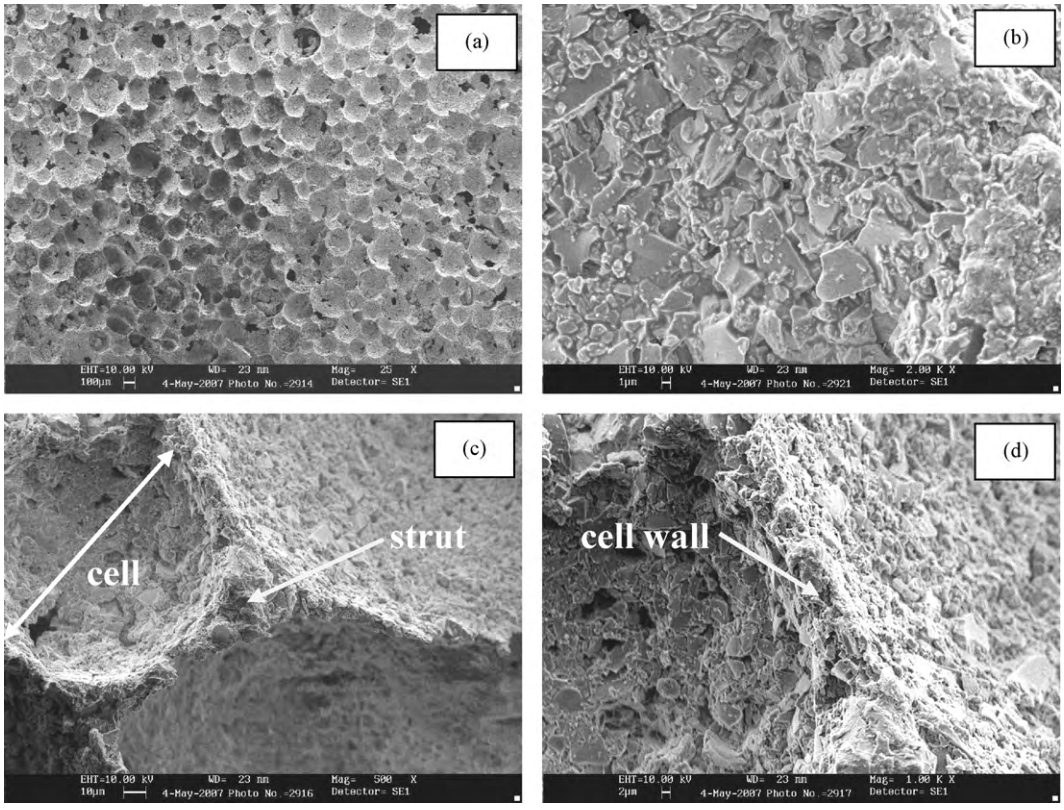

Fig. 5. SEM micrographs of silica foams with RD of 0.11 showing: (a) pore morphology at low magnification, (b) densification of cell wall, (c) a triangular strut, and (d) a single partition wall.

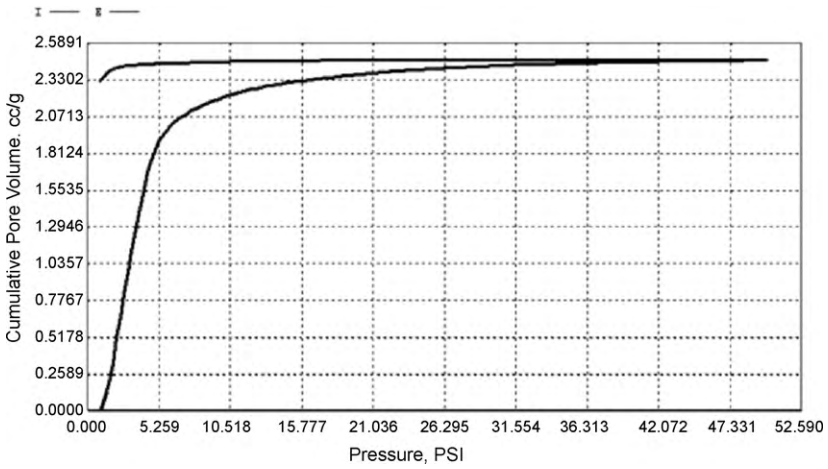

Fig. 6. Plot depicting the variation of the cumulative pore volume (net volume of displaced mercury) with pressure for sintered silica foam with optimum composition and RD = 0.11.

Table 1
Density and shrinkage data for silica foam panels.

Green body characteristics	
Density (apparent/RD)	0.225–0.27 (0.10–0.12)
Linear drying shrinkage (%)	4
Volume shrinkage (%)	23
Sintered body characteristics	
Relative density	0.105
Sintering shrinkage (%)	Negligible

It was observed under systematic experimental trials that although the slurries with solids loading of 30 and 32 vol.% both were shear thinning in nature, yet the consistency (k) is higher and the non-Newtonian index (n) is lower in the slurry with solids loading of 32 vol.%. In principle, a lower value of the 'n' of a slurry suggests its more shear thinning nature. Hence, the slurry with 32 vol.% of has been preferred for the optimum composition in lieu of its higher shear thinning nature (lower 'n') and consistency index (k), considering the pouring operation during processing.

3.2. Density and shrinkage

The photographs of the green panels (or tiles) made form the silica suspensions are shown in Fig. 3. The density, porosity content and volume shrinkage of both the green and sintered bodies are listed in Table 1. It was found that the process consistently yield a density of 0.368 ± 0.045 g/cc for wet foam samples and 0.248 ± 0.03 g/cc (relative density; RD = 0.11 ± 0.013) for the green bodies. Table 1 also shows that the relative density of the sintered foam (RD ~0.105) is very close to that of the green body, since the shrinkages during sintering are negligible.

3.3. Microstructural analysis

The pore morphologies and size distribution in the foams have been examined using optical and scanning electron microscopy aided by image analysis. The optical micrographs of silica foam samples with relative densities in the range of 0.11–0.2 have been shown in Fig. 4a and b.

The results obtained from the examination of optical micrographs (Fig. 4a and b) and from the use of linear intercept method to measure pore count illustrate that: (i) the foams with RD = 0.11 show uniform cell sizes, with an average pore count of ~10 pores per inch (ppi) (Fig. 4a), (ii) the average pore count in the case of foams with RD = 0.20 is found as ~16 ppi (Fig. 4b). It is therefore suggestive of that the increase in RD increases the pore count in the silica foam.

The microstructures of the silica foam samples with RD 0.11 are shown in the SEM micrographs depicted in Fig. 5(a–d). The densification of the silica foams with the increasing densities and the thickness of the struts (partition wall between air bubbles) contribute significantly to the mechanical strength and thermal

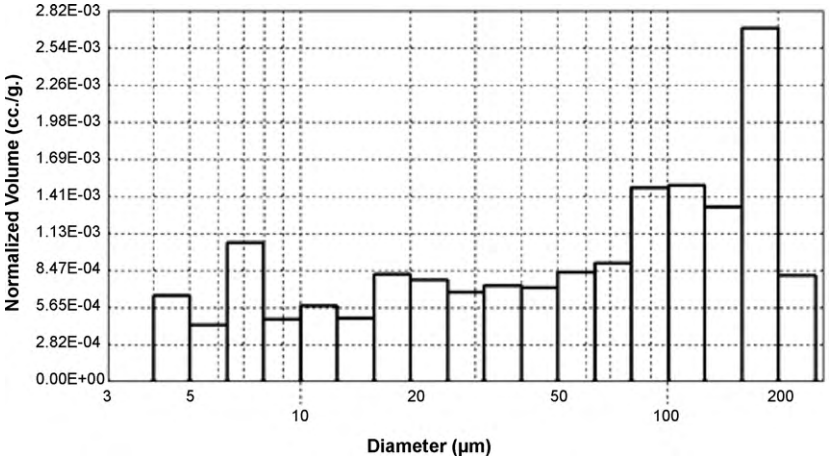

Fig. 7. Histogram of normalized volume as a function of pore diameter for sintered silica foam with optimum composition and RD = 0.11.

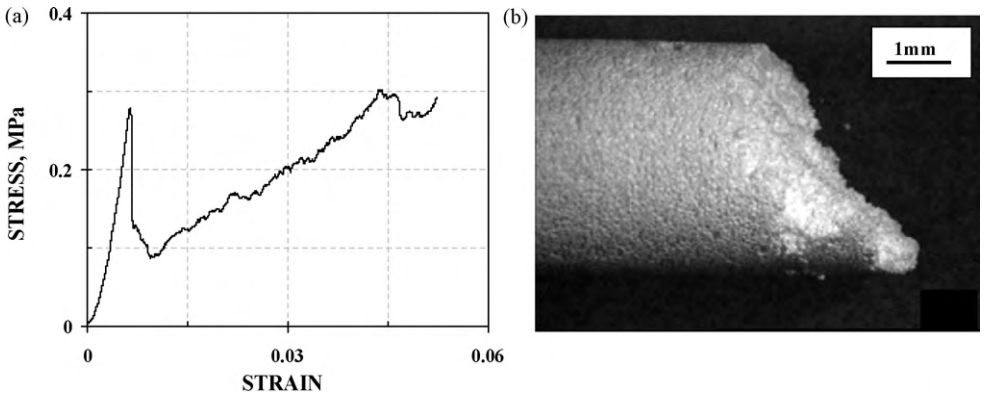

Fig. 8. Mechanical behavior of the foam (RD = 0.11) (a) a typical stress-strain curve under compression and (b) optical micrograph of the fractured foam surface.

properties of foams, as these are the load bearing and heat transfer regions in cellular ceramics. The microstructure has shown an open and interconnected porosity in foams with uniform pore (cell) size distribution. Examination of the pores (Fig. 5a) exhibits that the pores are nearly spherical and more uniformly distributed in the foams with RD = 0.11. The qualitative information from study of the cell walls in Fig. 5b exhibits that the cell walls are partially dense (absence of micropores), but the grains located in the cell wall are of different sizes and shapes. Measurements using the optical images (Fig. 5c) show that the average strut thickness is (i) ~4–5 μm in the foam with RD = 0.11 with a dense partition wall (Fig. 5d).

3.4. Mercury porosimetry

A plot depicting the variation of cumulative pore volume with pressure for the silica foam with RD = 0.11 (optimum composition) is shown in Fig. 6. The plot shows the cumulative volume of pores filled as the pressure is increased to a set maximum value and then decreased to zero. As expected, the cumulative pore volume increases with pressure because the mercury enters into smaller pores at high pressures. The histogram showing the bar charts for normalized pore volume (intrusion curve) with pore size distribution against the diameter for silica foams with RD = 0.11 is shown in Fig. 7. Analysis of the histogram in Fig. 7 leads to the following inferences: (i) the pore size distribution is wide with a range of 10–250 μm; and (ii) a relatively high volume fraction of pores lies in the range of 100–250 μm. In addition, since the cell walls

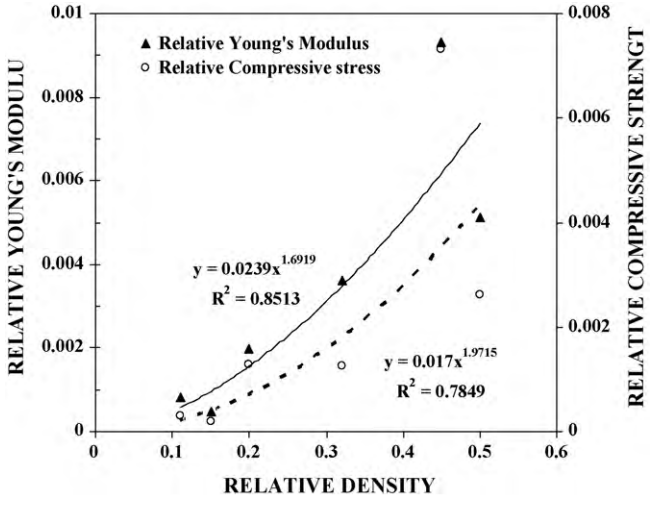

Fig. 9. Plots depicting the variation of relative Young's modulus and relative compressive strength as a function of relative density for open cell silica foams.

Table 2
The values of C_i, n and R^2 determined (present study) for the Young's modulus and compressive strength of *open cell* silica foams as a function of relative density.

Property	C_i	n	R^2
Young's modulus	0.024	1.69	0.85
Compressive strength	0.017	1.97	0.78

are also partially porous exhibiting the microporous tortuous channels within the cell walls and the struts (Fig. 5), the smaller pore sizes (5–50 μm) in the histogram (Fig. 7) represents the pores in the cell walls and the triangular struts whereas the bigger pores (100–250 μm) represent the cells.

3.5. Permeability

The values of permeability of the sintered foam samples (25 × 25 × 8 mm) as a function of the relative density, exhibits that the permeability decreases with the relative density of the porous body, as expected. For densities less than 30%, the permeability is ~10^{-8} m^2, whereas for the samples with 60% density, it is further reduced to 10^{-12} m^2.

3.6. Mechanical properties

A typical stress-strain curve for silica foams with 89 vol.% porosity (RD 0.11) is shown in Fig. 8a which shows that the foam samples exhibit mechanical behavior, typical of cellular materials. The compressive stress shows an initial linear elastic region, followed by a drop indicating cracking of some of the struts in the sample. Subsequently, further strain leads to the collapse of some of the cells with coming together of the cell walls, and increase in relative density. The coming together of cell walls as well as the support from unbroken struts provides support against the applied load, leading to increase in stress with displacement. As all the cell walls collapse, and begin to press against each other, the stress is expected to increase mainly, because the foam approaches the theoretical packing density of the material. The optical micrographs of the fractured foam surfaces are shown in Fig. 8b. It is clear from Fig. 8b that the failure has occurred at an angle to the applied stress axis, indicating the role of shear. Brittle materials are strong in uniaxial compression, but are weak in shear. This explains the cause for the failure of the foams under compressive stress along the plane of maximum shear. The silica foams produced for densities in the range of 11–62% have compressive strength and Young's modulus of ~0.28–3.3 and ~60–375 MPa, respectively.

In the present study, the geometric constant, C_i and the property dependent exponent, n of silica foams has been determined

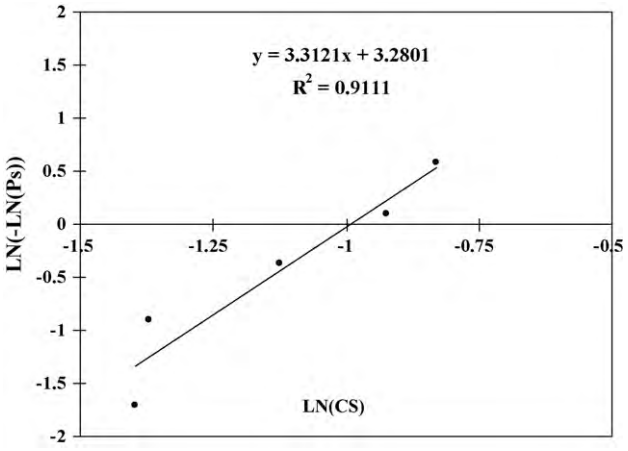

Fig. 10. Weibull plot for silica foams with RD = 0.11.

using Eq. (1), by iterative best fitting of the experimental data, for relative Young's modulus (ratio of Young's modulus of foams to that of the bulk, dense material) and relative compressive strength (ratio of compressive strength of the foam to that of the bulk matrix), respectively. The plots for the relative Young's modulus and relative compressive strength against the relative densities of silica foams are shown in Fig. 9 and the corresponding values of C_i, n and regression coefficient, R^2 obtained from Fig. 9 are given in Table 2. The cell wall material (fused silica in bulk form) properties such as Young's modulus (73 GPa) and compressive strength (1.108 GPa) have been used as reference values for the calculation of relative Young's modulus and relative compression strength of the silica foam samples with different relative densities (0.11–0.50).

The Weibull modulus values in the present study ranges from 2.4 to 7.2 for the foams with RD between 0.10 and 0.50. Figs. 10 and 11 show the weibull statistical plots for foams with RD between 0.10 and 0.20 showing the weibull modulus values ~3. As the Weibull modulus increases, the transition from probability of no failure to that of failure occurs more sharply and over a shorter range of stress. In other words, the scatter in the results of mechanical tests is reduced significantly, and failure prediction is more accurate. Hence, higher Weibull modulus is achieved in samples with a more uniform distribution of flaws.

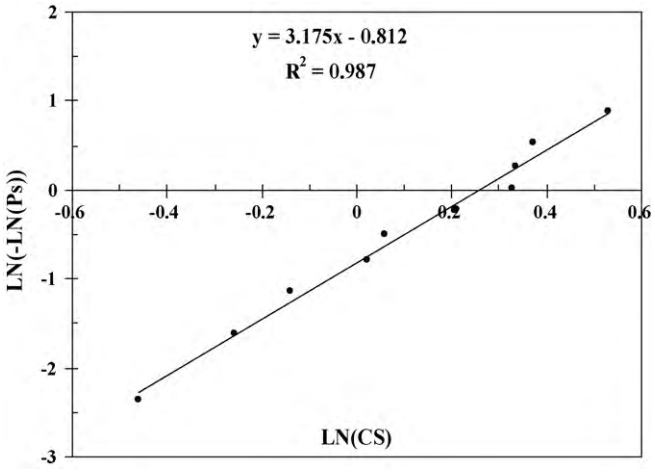

Fig. 11. Weibull plot for silica foams with RD = 0.20.

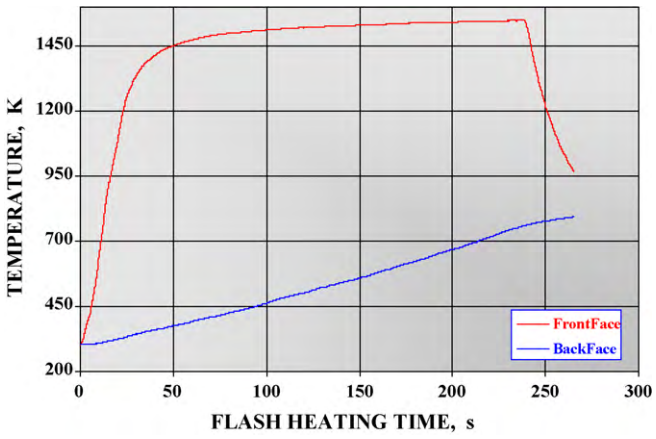

Fig. 12. Plots depicting the front and rear face temperatures of the porous silica tile as a function of time.

3.7. Thermal behavior

In the present study, the front surface of silica tiles with RD = 0.20 have been exposed to rapid heating, and the front and rear face temperatures are plotted as function of time in Fig. 12. The temperature profiles of the front and back faces clearly indicate that the porous silica tiles are stable up to 1550 K (1277 °C) with a rear face temperature of ~700 K (427 °C). Such a large difference between the front and back surfaces implies that the thermal insulation properties are impressive. Fig. 13 shows the plots depicting the profiles assuming different thermal diffusivities using a one-dimensional (1D) time marching solution [Eq. (2)].

The back face thermal profile of the silica tile determined experimentally in this study has been fitted against the calculated thermal profiles in Fig. 13. Comparison of the experimental curve with the calculated temperature profiles indicates that the thermal diffusivity (α) for the porous silica tile is ~0.55. Considering a bulk density of 450 kg/m^3 (since RD = 0.20) and specific heat of 740 J/kg K, and using the thermal diffusivity data, the thermal conductivity of the porous silica tile has been calculated as 0.18 W/m K, which is 1/8th that of bulk, dense fused silica. The source of experimental error in the approach for the measurement of thermal conductivity arises from the flow of heat in the plane of front face, in addition to that across the thickness.

Fig. 14 shows the X-ray radiograph (back face) of a thermal shock tested foam sample (RD = 0.14, 85 × 85 × 25 mm). Examina-

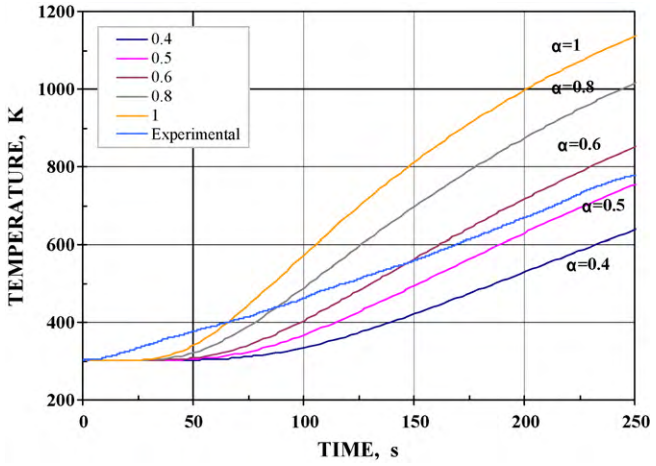

Fig. 13. Calculated thermal profiles assuming different thermal diffusivities using one-dimensional time marching solution.

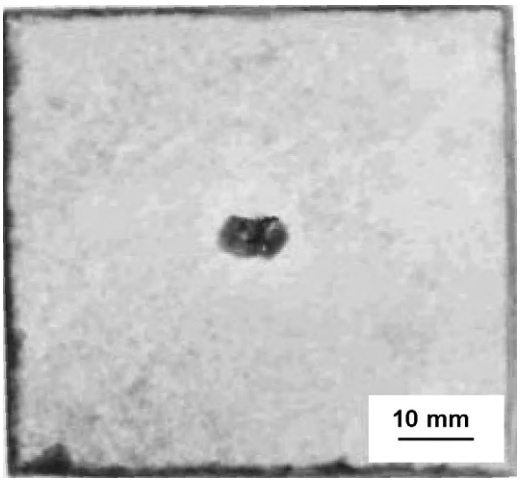

Fig. 14. X-ray radiograph of a thermal shock tested 100 × 100 × 25 mm silica tile. The back face of the tile is placed on the top.

tion of the radiograph does not show any evidence of variation in brightness or the X-ray transmittivity, except at the central spot appearing dark. The dark area at the center is caused by damage due to the exposure to the rapid heating by exposure to the flame. The sample shows almost no evidence of internal cracks after the exposure of the sample up to ~1500 K for the flash time of ~4 min. Cracks are, however expected as a result of the thermal residual stress caused by the presence of temperature gradient across the thickness of the porous silica tile.

Bar charts depicting the Young's modulus of the untested, coated and uncoated silica foams, exposed to thermal gradient (as in Fig. 12) are presented in Fig. 15 for comparison. The results show that the Young's modulus of the porous silica tiles decreases after the exposure to thermal gradient from 0.79 to 0.24 GPa, which is equivalent to a 3-fold reduction.

The reduction in the Young's modulus is obviously due to the damage at the center of the tile (shown in Fig. 14), and is also suggestive of the occurrence of the internal defects due to the generation of thermal stresses while testing. Since the X-ray radiograph has not shown any evidence of discontinuities across the thickness of the tiles, it is expected that microcracks are formed and those are beyond the resolution limit of X-ray radiography.

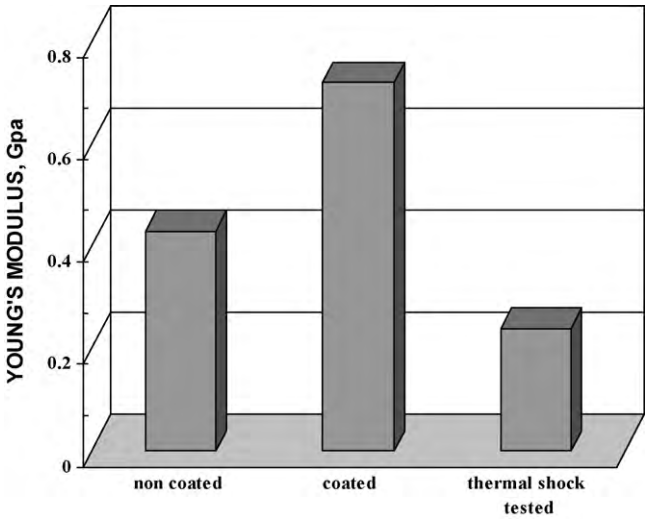

Fig. 15. Bar charts depicting the effect of thermal shock on the young's modulus of the silica tiles.

4. Summary and conclusions

A novel approach for producing the ceramic foams from inexpensive silica powder has been developed. The pores produced with this approach result from the direct entrainment of air bubbles into a ceramic suspension. The different processing parameters that control the final properties of foams have been optimized. Panels with thickness of 25–30 mm have been dried under controlled humidity without cracking, and with uniform linear shrinkage of 10%. Silica foams having high structural integrity, nearly spherical pores with an average size of 250 μm, interconnected porosity, and possessing as low as ~11% density, have been successfully fabricated. The permeability, elastic modulus and the compressive strength of the porous silica tiles are a function of the foam density. The silica foams thus produced, have strength levels in the range of ~0.28–3.3 MPa, for densities in the range of 11–62%. The low values of thermal diffusivity and conductivity, which are due to the presence of large volume percent of tailored porosities, make the silica foams suitable for use in the thermal insulation tiles, meant for protection against degradation during exposure at elevated temperatures.

Impact of this study

The porous silica tiles prepared through the present study offer many advantages:

i. Silica tiles with relative density of 0.15 and approximate thermal conductivity (through the thickness) of ~0.18 W/m K have been developed.
ii. The low Young's modulus of the porous silica tiles lowers the thermal residual stress and thermal shock problems.
iii. Since the powder composition and sintering parameters [10] have been carefully optimized, conversion to the crystalline phase, cristobalite could be limited and hence, the stresses associated with volume change are reduced.
iv. Since the surfaces of porous silica tiles have been densified with silica [10], both the handling strength as well as the ability to maintain structural integrity is improved. The later is attributed to the absence of mismatch in the coefficients of thermal expansion between the foam and the coating.

Acknowledgment

The authors are thankful to Defence Research & Development Organization (DRDO) for the financial support for this work.

References

[1] L.J. Korb, C.A. Morant, R.M. Calland, C.S. Thatcher, Ceram. Bull. 60 (1981) 1188–1193.
[2] K.J. Korb, H.M. Claney, Proceedings of the 26th National SAMPE Symposium, Los Angeles, USA, 1981, pp. 232–249.
[3] D.B. Leiser, M. Smith, H.E. Goldstein, Ceram. Bull. 60 (1981) 1201–1204.
[4] P. Sepulveda, Am. Ceram. Soc. Bull. 76 (10) (1997) 61–65.
[5] M. Scheffler, P. Colombo, Cellular Ceramics—Structure, Manufacturing and Applications, Wiley VCH, Germany, 2005, pp. 291–310.
[6] J.S. Woyansky, C.E. Scott, W.P. Minnear, Am. Ceram. Soc. Bull. 71 (11) (1992) 1674–1682.
[7] H.N. Wang, P. Yuan, L. Zhou, Y.N. Guo, J. Zou, A.M. Yu, G.Q. Lu, C.Z. Yu, J. Mater. Sci. 44 (2009) 6484–6489.
[8] F. Carn, A. Colin, M-.F. Achard, H. Deleuze, Z. Saadi, R. Backov, Adv. Mater. 16 (2004) 140–144.
[9] A.R. Studart, U.T. Gonzenbach, E. Tervoort, L.J. Gauckler, J. Am. Ceram. Soc. 89 (6) (2006) 1771–1789.
[10] S. Mishra, R. Mitra, M. Vijayakumar, J. Eur. Ceram. Soc. 28 (2008) 1769–1776.
[11] ASTM International, Standard Test Method for Permeability of Refractories. C 577-99 (1999) 99–102.
[12] R. Brezny, D.J. Green, Uniaxial strength behavior of brittle cellular materials, J. Am. Ceram. Soc. 76 (1993) 2185–2192.
[13] J.S. Reed, Principles of Ceramic Processing, 2nd ed., John Wiley and Sons, Inc, New York, 1988, p. 283.